RSC Advances

PAPER

View Article Online
View Journal | View Issue

Cite this: *RSC Adv.*, 2017, **7**, 44234

Robust superhydrophobic coatings with micro- and nano-composite morphology†

Jitong Li, Lei Zhou, Nan Yang, Chunlei Gao and Yongmei Zheng *

Received 15th August 2017
Accepted 31st August 2017

DOI: 10.1039/c7ra09016a

rsc.li/rsc-advances

A robust superhydrophobic coating (SC) surface can be fabricated by the sol–gel processing of long-chain 3-methacryloxypropyltrimethoxysilane and fluorosilanization by CVD. The SC surface is formed with a unique micro- and nano-composite morphology similar to that of a lotus leaf. As a result, it displays strong liquid repellency (*e.g.*, water, brine, acidic solutions). In particular, the SC on a glass surface displays high transmission of light, robust UV durability, weather resistance, strong binding adhesion, and excellent scratch-resistant properties.

Superhydrophobic coatings have received increasing attention in basic and applied research in important areas, *e.g.*, self-cleaning,[1–4] antifogging and snow prevention,[5,6] anticorrosion and corrosion resistance,[7,8] anti-icing,[9–12] and others.[13,14] As is well known, many surfaces of plants and animals (*e.g.*, lotus leaf, water strider legs, butterfly wings) have superhydrophobic properties, attributed to roughness and to waxes present on the surfaces[15,16] and to cooperation between micro- and nano-structures.[17,18] To obtain superhydrophobic coatings, a range of methods have been developed, *e.g.*, dip-coating,[19,20] sol–gel process,[21,22] chemical etching,[23,24] spin-coating,[25,26] plasma treatment,[27] electro-spinning,[28,29] and layer-by-layer (LBL) assembly;[30,31] thus some significant advances have been made. For instance, Mahadik *et al.*[21] demonstrated a simple dip coating method for the preparation of superhydrophobic films on a glass substrate at room temperature by the sol–gel process. Seo *et al.*[32] created a transparent superhydrophobic coating through the use of silicone oil and controlled combustion. Wang *et al.*[33] fabricated a stable bionic superhydrophobic surface by immersing a copper plate into a solution of fatty acid. Zheng *et al.*[34] used the chemical vapor deposition method to prepare a polyvinylidene fluoride (PVDF) coating with smooth and regular surface structures, and then treated it with NaOH solution and finally fabricated the super-hydrophobic surface. Givenchy *et al.*[35] treated a rough PDMS surface with sulfuric acid or hydrofluoric acid, and then combined it with a per-fluorinated molecular membrane to obtain a super-hydrophobic surface. Ye *et al.*[36] constructed a fluorine-free and cost-effective superhydrophobic surface with normal-alcohol-modified hydrophobic SiO_2 nanoparticles. Up to now, it still remains challenging to address problems such as UV durability and strong binding adhesion.

Here, we present a kind of superhydrophobic coating (SC) that can be fabricated by the sol–gel processing of long-chain 3-methacryloxypropyltrimethoxysilane and fluorosilanization by CVD. It was found that the SC surface can be formed with a unique micro- and nano-composite morphology similar to that of a lotus leaf. We further demonstrate that the SC surface display strong liquid repellency (*e.g.*, water, brine, acidic liquids), in addition to the high transmission of light, robust UV durability, weather resistance, strong binding adhesion and excellent scratch-resistant properties. The study is significant for the design of coatings that can be extended to applications such as self-cleaning, anti-abrasion, anti-corrosion, and water-proofing.

In this study, silicon dioxide was combined with 3-meth-acryloxypropyltrimethoxysilane by sol–gel processing and fluo-rosilanization by CVD to prepare the superhydrophobic coatings on glass. Silica is a material with good compatibility with stone and it has good acid resistance. A large number of hydroxyl groups exist on the porous inner surface of the nano-silica coating, which is the cause of the hydrophilicity of nano-silica. Therefore, the reactive hydroxyl groups are replaced through the surface modification process, which is a way to achieve the hydrophobicity of the coating. It is known that superhydrophobic surfaces are made up of multilevel rough surfaces with micro/nano structures combined with low surface energy material (*e.g.* waxy crystals). It has been proved that the coexistence of surface roughness and low surface energy material are prerequisites for achieving super-hydrophobicity.[18,37] From the main influencing factors of surface wetting, herein, the surface roughness is increased and the surface energy is lowered to enhance the hydrophobicity of the surface.

In view of the influence of the chemical components of the surface on the wettability, elemental analysis of the SC surface was carried out using X-ray photoelectron spectroscopy (XPS).

School of Chemistry, Beihang University, Xueyuan Road 37, Haidian District, Beijing, 100191, China. E-mail: zhengym@buaa.edu.cn

† Electronic supplementary information (ESI) available. See DOI: 10.1039/c7ra09016a

In the XPS spectrum, the abscissa represents the binding energy of each element and the ordinate denotes the intensity of the photoelectrons. Different atoms have their characteristic binding energies; the elemental composition of the surface and the state of existence of each element can be determined according to the location of the peaks in the XPS diagram. Fig. 1a shows the broad XPS spectrum of the SC surface. Note that the obtained binding energies of 102.1, 290.5, 520.7, and 691.2 eV denote the existence of Si, C, O, and F, respectively. The relative mass fractions (atomic%) are 19.95%, 25.69%, 40.40%, and 13.96%, respectively. The C 1s peak is attributed to the C–H bonds in the $-CH_2-$ and $-CH_3$ groups. O 1s is clearly the C–O bond, and the Si 2p peak is consistent with the binding energy.[38] The inset shows the high-resolution XPS spectrum of F 1s, with the characteristic absorption peak of fluorine at 691.2 eV. The characteristic C 1s peaks at 289.1 and 292.2 eV are attributed to CF_2 and CF_3, respectively, which is consistent with the components of FAS ($C_{16}H_{19}F_{17}O_3Si$).

The microstructure of the SC surface was observed by scanning electron microscopy (SEM). Fig. 1b and c show the SEM images of the SC surface, which is composed of nano-scaled protrusions and nanoparticles in the range of 40–100 nm. The granules are dispersed on the surface to form the nano-structure. Micro-level aggregates also exist, which is due to the fact that a proportion of the nano-silica particles are reunited in the spraying and heat curing process. The image confirms that there is little porosity in the microstructure of the polymer, which indicates that the fluorinated precursor is well mixed within the polymer matrix and many of the particles are cross-linked together. Fig. 1d and e show the two- and three-dimensional atomic force microscopy (AFM) images of the SC surface, respectively. The scanning region is 5 μm × 5 μm and the *Z*-axis has a maximum protrusion of 192.1 nm (Fig. 1d). The AFM analysis indicates roughness with a root mean square (RMS) of 77.8 nm (Fig. 1e). Many large humped structures exist on the surface of the coating, resulting in a further increase of the roughness.

The surface is mainly composed of closely packed nanoparticles and scattered dense hill-shaped bulges, indicating that the coating has a lotus-like micro–nano-structure. This special structure gives the coating superhydrophobic properties. Fig. 1f shows the fluctuated height graph of a linear region in the AFM image (Fig. 1e). Analysis indicates an average roughness (R_a) of 95.21 nm. Combining low surface-energy material with dual-scaled (micro and nano) surface roughness is essential for superhydrophobic surfaces.[17]

It is known that a larger contact angle is related to the better hydrophobicity of a surface with low surface energy and high geometric roughness. According to the Wenzel equation:[39] $\gamma_{LA}\cos\theta_\omega = r(\gamma_{SA} - \gamma_{SL})$, where θ_ω is the apparent contact angle of the liquid on a rough surface; γ_{LA}, γ_{SA}, and γ_{SL} are tensions of the liquid–air, solid–air, solid–liquid interfaces, respectively; and r is the roughness of the surface. The high roughness makes the hydrophobic surface more hydrophobic for a low surface-energy material surface. Wettability was examined on the SC surface, where the static water contact angle on the glass substrate was 161.2°, the brine contact angle was 151.3°, the contact angle of CH_2Cl_2 : H_2O in a molar ratio of 1 : 20 was 155.2°, and the contact angle of CH_2O_2 : H_2O in a molar ratio of 1 : 20 was 147.4° (see insets of Fig. 2a–d, photos of droplets). The liquid repellence can be observed subsequently on the SC surface. Fig. 2a shows the water droplet bouncing process on the SC surface. The water droplet completely rolls off the surface without wetting, showing outstanding water repellence and indicating that the surface is superhydrophobic. Correspondingly, we also carried out the droplet bounce experiments for brine (Fig. 2b), CH_2Cl_2 : H_2O in a molar ratio of 1 : 20 (Fig. 2c) and CH_2O_2 : H_2O in a molar ratio of 1 : 20 (Fig. 2d). It can be seen that the four droplets have similar bounce properties (see ESI Movies S1–S4†). Among them, the water and brine droplets bounce very high, and can be separated from the surface and have a second bounce, unlike the CH_2Cl_2 and CH_2O_2 droplets (Fig. S2, see ESI Movies S5 and S6†). Although their surface tension increases when they are mixed with water at a molar ratio of 1 : 20, they also can achieve bouncing. The adhesion of

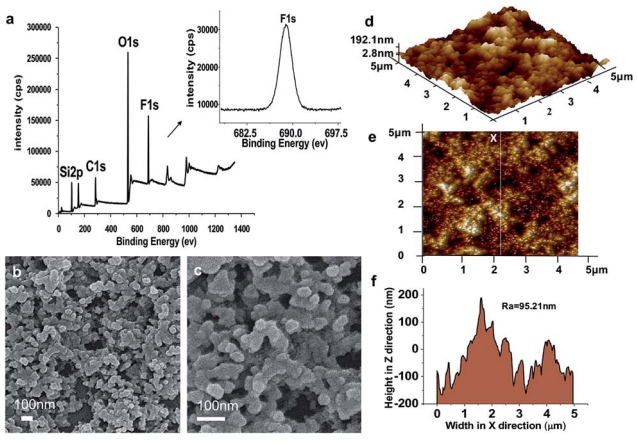

Fig. 1 (a) XPS spectrum of SC surface. The inset is a high-resolution F 1s spectrum of the coating, where "F" refers to FAS. (b, c) SEM images of SC surface. (d, e) 3D and 2D AFM images of SC surface. (f) Analysis of AFM in the average roughness (R_a = 95.21 nm) of the linear region corresponding to (e).

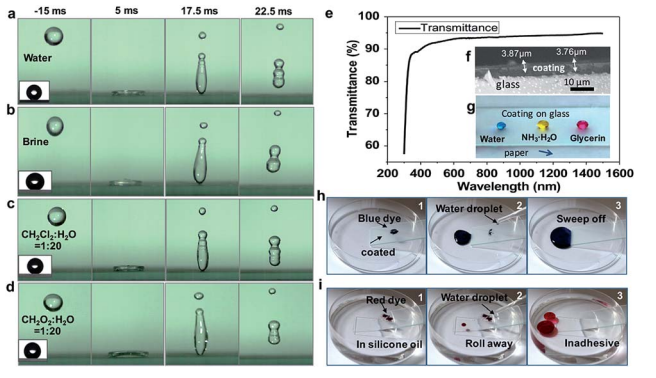

Fig. 2 (a–d) Bouncing on SC surface (insets are photos of droplets like balls). (e) Transmittance spectra of SC surface. (f) SEM image of SC surface with thickness of 3.7–3.8 μm. (g) Optical image of water droplet (blue), $NH_3\cdot H_2O$ (yellow) and glycerol (red) on the coating. (h, i) Self-cleaning properties of SC surfaces.

the surface can be estimated by observing a droplet sliding off the surface. A 5 μL water droplet was placed on the SC surface and the surface was slowly inclined. A sliding angle of ~4° was observed for the water droplet (Fig. S3, and see also ESI Movie S7†). It can be estimated that the SC surface has the very low adhesive force of 31.9 μN, so that the water droplet can easily roll away. In addition, we also tested the adhesion of ammonia and glycerol, *i.e.*, 41.8 μN and 51.1 μN, respectively.

To demonstrate the SC in the visible spectrum, we prepared the coating at a thickness of 330 ± 40 nm on a glass substrate. The wavelength of the light in the test was in the range of 400–1500 nm. As shown in Fig. 2e, the transmission of light in the visible range of the spectrum is ~90%. Fig. 2f shows the cross section of the coating; the thickness of the coating is about 3–4 μm. Fig. 2g shows optical images of droplets on the SC surface. Blue dye represents water droplets, yellow dye is $NH_3 \cdot H_2O$, and red dye is glycerol. The SC on glass would be higher transparency. It demonstrates that the size of the SiO_2 particles, the thickness of the coating and the SiO_2 content% can be optimized to achieve the excellent transparency of the coating (see Fig. S4 and 5†).

Self-cleaning performance is one of the most important properties of superhydrophobic coatings, and is crucial for some applications.[40–42] In order to characterize the self-cleaning performance, contaminant powders were uniformly spread on the SC surface and bare glass. The self-cleaning process is shown in Fig. 2h, where water droplets can easily roll off the inclined surface. After several cycles, the water droplets adsorb the contaminants completely and leave the self-cleaning trajectory (see ESI Movie S8†). Fig. 2i shows the dye removal at the oil–solid–vapor interface; water droplets are dropped onto the surface and remove the dirt both in the air and in the oil. The SC surface exhibits excellent self-cleaning performance (see ESI Movie S9†).

Wettability was examined by water contact angles with different droplet sizes. Fig. 3a shows that the contact angle changes with droplet size. The contact angle exhibits a downward trend when the water droplet becomes larger. However, all the contact angles are in excess of 150° and the coating has excellent hydrophobicity. Fig. 3b shows water contact angles of the SC surface at different ultraviolet aging times of 15, 30, 90, and 150 min. The contact angle does not change significantly with increasing UV exposure time (the experimental wavelength range is 320–450 nm), indicating that the coating can stably maintain its superhydrophobicity. Fig. 3c shows the water contact angles of the SC surface at different aging times of 2, 4, 6, 8, and 10 days in the outdoor haze environment. The contact angle of water remained above 150° for over 10 days, demonstrating the superhydrophobicity of the surface. In addition, the coating also shows high resistance against droplets in the outside environment, high temperature, and acidic conditions, *etc.* (Fig. S6†). Fig. 3d shows that the contact angle varies with the ratio of formic acid to water. When the formic acid drops on the SC surface, it presents a hydrophilic state. However, when the formic acid droplets are mixed with water, and then dropped on the SC surface, it shows a state of hydrophobicity. In addition to formic acid, similar phenomena were observed with acetic acid, dichloromethane, cyclohexane and *n*-hexane. The surface tension of water is 72.8 mN m^{-1} and the surface tension of organic liquids is less than that of water. At room temperature, most of the liquid surface tensions are in the range of 20–40 mN m^{-1}. From the photos in the insets (Fig. 4e), it can be seen that when the surface tension of the gas–liquid interface increases, the contact angle increases correspondingly. Thereby, as the surface tension increases, the contact angle increases when adding different proportions of water to formic acid.

Abrasive resistance is an important measure of the mechanical strength of the coating and is also one of the important indexes indicating the performance of the coating.[43–45] In general, superhydrophobic coatings are not mechanically stable, owing to their high surface roughness, and

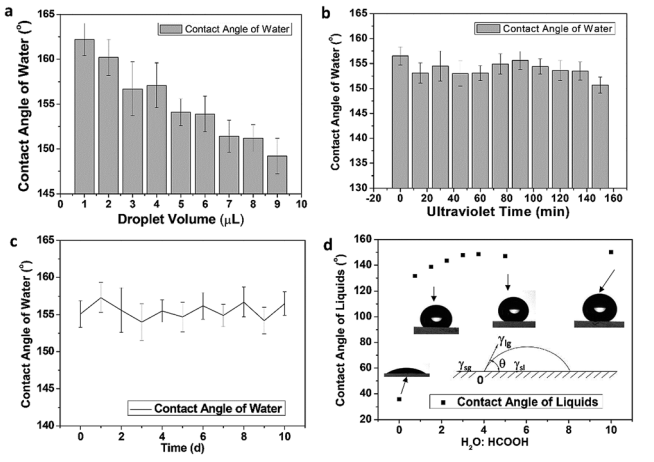

Fig. 3 (a) Contact angle changes with different droplet sizes. (b) Water contact angles of SC surfaces at different ultraviolet aging times of 15, 30, 90, and 150 min. (c) Water contact angles of SC surface at different aging times of 2, 4, 6, 8 and 10 days in the outdoor haze environment. (d) The contact angle varies with the ratio of formic acid to water.

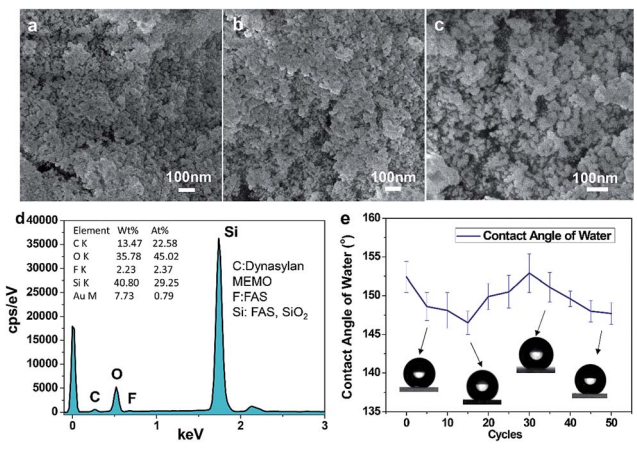

Fig. 4 (a–c) SEM images after 50 cycles of sandpaper abrasion friction on the SC surface with magnification of (a) 40 000×; (b) 50 000×; and (c) 70 000×. (d) The EDS spectrum of the elements contained in SC. (e) Water contact angles after abrasion (inset images show corresponding water contact angles).

they are susceptible to damage from mechanical friction. In this experiment, we used Dynasylan MEMO to combine with the substrate better in the ultraviolet curing conditions, which improved the wear resistance. In order to verify the abrasive resistance of the SC, we rubbed the superhydrophobic surface with sandpaper. Fig. 4a–c show the SEM images of the SC surface after 50 sandpaper abrasion cycles. The surface shows a network-like structure and the interior is still filled with voids (Fig. 4c). A large number of micropores and protrusions remain on the surface. The analysis of the elemental content in SC after friction is shown in Fig. 4d, where the major chemical elements contained in the coating did not change after rubbing. After 50 sandpaper abrasion cycles, the contact angle of the SC surface was maintained at about 146°, indicating the excellent hydrophobicity of the coating (Fig. 4e). The micro–nanostructure helps the coating to remain superhydrophobic. In addition, the hardness of the coating was also tested by the pencil hardness method, which showed a hardness of 1H.

Conclusions

In conclusion, we have successfully fabricated a superhydrophobic coating (SC) that is robust, scratch-resistant, self-cleaning, and optically transparent. The SC surface exhibits a rough, wrinkled, hill-like surface morphology, and the liquid droplets (*e.g.*, water, brine, acidic liquids) present a spherical shape, along with a high contact angle and low sliding angle, rebounding upon the SC surface. Various droplets of water, brine, and acidic liquids can bounce upon the SC surface, which displayed strong liquid repellency. Light transmission can be induced on SC over glass. In particular, the coating shows a high resistance against droplets, strong binding adhesion, and durability against UV and the outside environment. It opens a new way to design coating materials that can be extended to practical applications in fields such as self-cleaning, anti-abrasion, anti-corrosion, and water-proofing.

Conflicts of interest

There are no conflicts to declare.

Acknowledgements

The work is supported by National Natural Science Foundation of China (21234001, 21473007, 21771015).

Notes and references

1 A. Nakajima, K. Hashimoto, T. Watanabe, K. Takai, G. Yamauchi and A. Fujishima, *Langmuir*, 2000, **16**, 7044.
2 Y. Lai, Y. Tang, J. Gong, D. Gong, L. Chi, C. Lin and Z. Chen, *J. Mater. Chem.*, 2012, **22**, 7420.
3 F. Arianpour, M. Farzaneh and S. A. Kulinich, *Appl. Surf. Sci.*, 2013, **265**, 546.
4 Q. Xu, J. Wang and K. D. Sanderson, *J. Mater. Chem.*, 2010, **20**, 5961.
5 S. A. Kulinich, S. Farhadi, K. Nose and X. W. Du, *Langmuir*, 2011, **27**, 25.
6 G. Wang, L. Zhu, H. Liu and W. Li, *Mater. Lett.*, 2011, **65**, 3095.
7 C. F. Carlborg and W. V. D. Wijngaart, *Langmuir*, 2011, **27**, 487.
8 K. Chang, H. Lu, C. Peng, M. Lai, S. Hsu, M. Hsu, Y. Tsai, C. Chang, W. Hung, Y. Wei and J. Yeh, *ACS Appl. Mater. Interfaces*, 2013, **5**, 1460.
9 L. Mishchenko, B. Hatton, V. Bahadur, J. A. Taylor, T. Krupenkin and J. Aizenberg, *ACS Nano*, 2010, **4**, 7699.
10 M. Ruan, W. Li, B. Wang, B. Deng, F. Ma and Z. Yu, *Langmuir*, 2013, **29**, 8482.
11 S. A. Kulinich and M. Farzaneh, *Cold Reg. Sci. Technol.*, 2011, **65**, 60.
12 L. Cao, A. K. Jones, V. K. Sikka, J. Wu and D. Gao, *Langmuir*, 2009, **25**, 12444.
13 Z. Xiong, H. Lin, Y. Zhong, Y. Qin, T. Li and F. Liu, *J. Mater. Chem. A*, 2017, **5**, 6538.
14 N. Wang, Y. Lu, D. Xiong, C. J. Carmalt and I. P. Parkin, *J. Mater. Chem. A*, 2016, **4**, 4107.
15 W. Barthlott and C. Neinhuis, *Planta*, 1997, **202**, 1.
16 C. Neinhuis and W. Barthlott, *Ann. Bot.*, 1997, **79**, 667.
17 L. Feng, S. Li, Y. Li, H. Li, L. Zhang, J. Zhai, Y. Song, B. Liu, L. Jiang and D. Zhu, *Adv. Mater.*, 2002, **14**, 1857.
18 S. Wang and L. Jiang, *Adv. Mater.*, 2007, **19**, 3423.
19 D. Mullangi, S. Shalini, S. Nandi, B. Choksi and R. Vaidhyanathan, *J. Mater. Chem. A*, 2017, **5**, 8376.
20 F. Chen, J. Song, Y. Lu, S. Huang, X. Liu, J. Sun, C. J. Carmalt, I. P. Parkin and W. Xu, *J. Mater. Chem. A*, 2015, **3**, 20999.
21 S. A. Mahadik, M. S. Kavale, S. K. Mukherjee and A. Venkateswara Rao, *Appl. Surf. Sci.*, 2010, **257**, 333.
22 X. Wu, Q. Fu, D. Kumar, J. W. C. Ho, P. Kanhere, H. Zhou and Z. Chen, *Mater. Des.*, 2016, **89**, 1302.
23 M. Qu, B. Zhang, S. Song, L. Chen, J. Zhang and X. Cao, *Adv. Funct. Mater.*, 2007, **17**, 593.
24 K. Li, X. Zeng, H. Li and X. Li, *Appl. Surf. Sci.*, 2015, **346**, 458.
25 S. G. Lee, D. S. Ham, D. Y. Lee, H. Bong and K. Cho, *Langmuir*, 2013, **29**, 15051.
26 R. Campos, A. J. Guenthner, A. J. Meuler, A. Tuteja, R. E. Cohen, G. H. Mckinley, T. S. Haddad and J. M. Mabry, *Langmuir*, 2012, **28**, 9834.
27 D. Han and S. Y. Moon, *Thin Solid Films*, 2015, **587**, 34.
28 A. Baji, M. Abtahi and S. Ramakrishna, *J. Nanosci. Nanotechnol.*, 2014, **14**, 4781.
29 H. Wang, H. Zhou, H. Niu, J. Zhang, Y. Du and T. Lin, *Adv. Mater. Interfaces*, 2015, **2**, 1400506.
30 L. Zhang, H. Chen, J. Sun and J. Shen, *Chem. Mater.*, 2007, **19**, 948.
31 Y. Li, F. Liu and J. Sun, *Chem. Commun.*, 2009, 2730.
32 K. Seo, M. Kim, S. Seok and D. H. Kim, *Colloids Surf., A*, 2016, **492**, 110.
33 S. Wang, L. Feng and L. Jiang, *Adv. Mater.*, 2010, **18**, 767.
34 Z. Zheng, Z. Gu, R. Huo and Z. Luo, *Appl. Surf. Sci.*, 2010, **256**, 2061.

35 E. P. T. de Givenchy, S. Amigoni, C. Martin, G. Andrada, L. Caillier, S. Geribaldi and F. Guittard, *Langmuir*, 2009, **25**, 6448.
36 H. Ye, L. Zhu, W. Li, H. Liu and H. Chen, *ACS Appl. Mater. Interfaces*, 2016, **9**, 858.
37 H. Meng, S. Wang, J. Xi, Z. Tang and L. Jiang, *J. Phys. Chem. C*, 2008, **112**, 11454.
38 E. Paparazzo, *Surf. Interface Anal.*, 1996, **24**, 729.
39 R. N. Wenzel, *Ind. Eng. Chem.*, 1936, **28**, 988.
40 S. Liu, X. Liu, S. S. Latthe, L. Gao, S. An, S. S. Yoon, B. Liu and R. Xing, *Appl. Surf. Sci.*, 2015, **351**, 897.
41 X. Zhang, Y. Guo, Z. Zhang and P. Zhang, *Appl. Surf. Sci.*, 2013, **284**, 319.
42 D. Zhi, Y. Lu, S. Sathasivam, I. Parkin and X. Zhang, *J. Mater. Chem. A*, 2017.
43 Z. Zhang, B. Ge, X. Men and Y. Li, *Colloids Surf., A*, 2016, **490**, 182.
44 Y. Lu, S. Sathasivam, J. Song, C. R. Crick, C. J. Carmalt and I. P. Parkin, *Science*, 2015, **347**, 1132.
45 J. Liang, L. Wang, J. Bao and L. He, *J. Mater. Chem. A*, 2015, **3**, 20134.